FAILURE MORPHOLOGY AND ENERGY ABSORPTION OF PREPREG PLATELET MOLDING COMPOUND TUBES

Rebecca A. Cutting, Johnathan E. Goodsell, R. Byron Pipes
Composites Manufacturing and Simulation Center, Purdue University, West Lafayette, IN 47906

Abstract

In recent years, carbon fiber composites have shown promise in the automotive industry because of their energy absorption capabilities. The most common composite energy absorbers examined have been tubes made of braided and continuous fibers with various cross sectional geometries. While a considerable amount of experimental work has looked at the effect of processing conditions and geometry on energy absorption, little work has been done to investigate the effect of fiber form on crush response in carbon fiber tubes. This work characterizes the failure morphology and energy absorption of circular tubes made from the thermoset prepreg platelet molding compound (PPMC) VORAFUSE M6400™ and compares the response to continuous fiber failures of the same material system. PPMC tubes displayed a failure morphology similar to that of a splaying failure mode seen in continuous fiber tubes, but the splaying segments were significantly larger. The load-displacement curves were similar in shape to those seen in the continuous fiber fragmentation mode. The average specific energy absorption of the PPMC tubes was less than 1 kJ/kg lower than the specific energy absorption of two different unidirectional layups made with the same material.

Introduction and Background

A significant amount of research has investigated the progressive crush response of continuous fiber composite tubes. Experimental testing of structural components for crash response in compression generally has three outputs of interest: failure morphology, load-displacement curve, and specific energy absorption.

Continuous Fiber Failure Morphologies

Hull [1], Farley, and Jones [2] are well known authors for their thorough investigations of failure morphology in composite crush tubes. Both sets of authors chose to look at hollow tubes with circular cross sections comprised of continuous fiber layups. From their investigations, there are four failure morphologies associated with the progressive failure of continuous fiber composite tubes. These are the splaying mode, the fragmentation mode, the brittle fracture mode, and the local buckling mode. Figure 1 provides a visual representation of each of these failure modes.

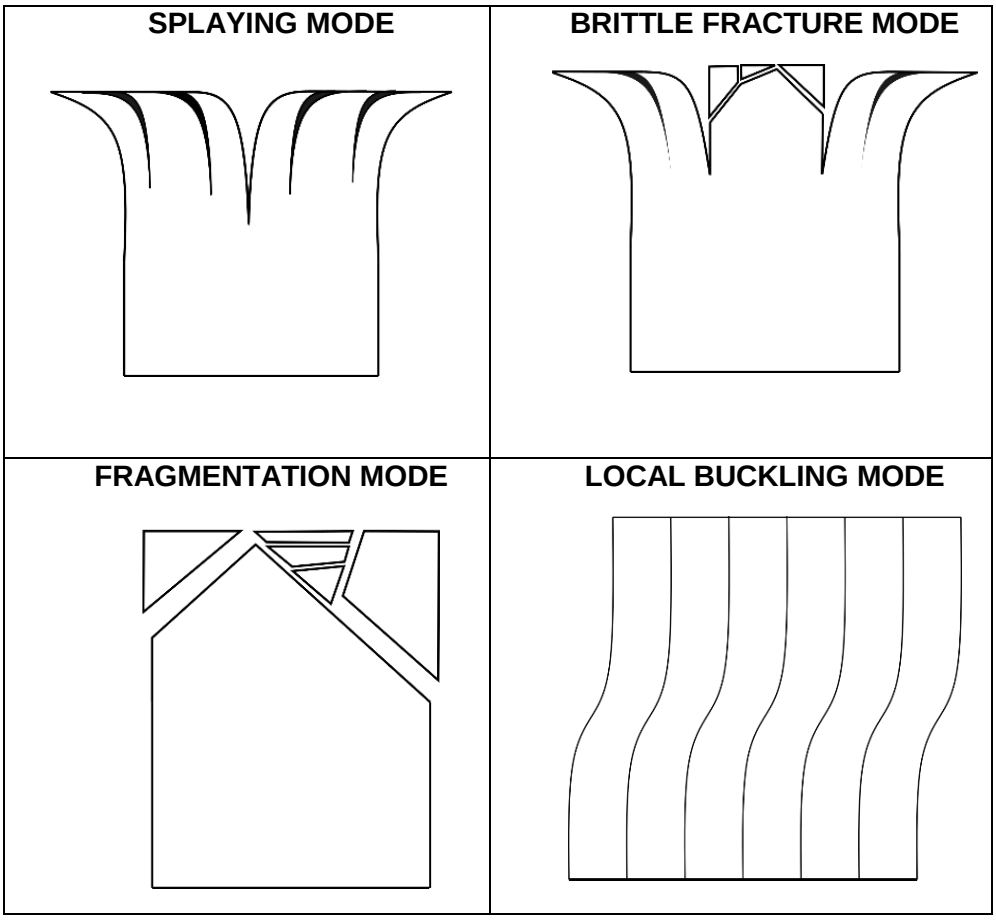

Figure 1: Failure morphology representations reproduced from work by Hull [1] and Farley [2]

The splaying mode appears when there is a high ratio of axial fibers within the laminate of the tube. Interlaminar cracks develop along with a wedge of debris that helps sustain the delamination process between plies. Most of the energy absorption comes from the crack growth in the delamination process.

The fragmentation mode is characterized by short interlaminar cracks that form lamina bundles. These bundles then fracture and break off from the tube walls. This mode is present when there is a high ratio of hoop fibers within the laminate. The energy absorption for this failure mode comes primarily from the fracturing of the bundles away from the tube wall.

The brittle fracture mode was only described by Farley, and is a combination of the splaying and fragmentation modes. Interlaminar cracks form within the laminate as well as fractured lamina bundles. The lengths of the interlaminar cracks can be up to ten times larger than those present in the fragmentation mode. However, these interlaminar cracks are still smaller than the interlaminar cracks present in the splaying mode.

The local buckling mode is the failure mode most commonly associated with ductile metals and aramid fiber composites. Plastic yielding of the fiber and matrix forms localized buckles that then stack on top of one another, eventually creating an accordion shape. This effect would not be possible without the formation of interlaminar cracks at the buckles themselves.

There is a large gap in literature with regards to crash performance of discontinuous carbon

fiber material systems, particularly prepreg platelet molding compound. A research group at Oak Ridge National Lab performed crush tests on chopped fiber prepreg material systems. However, they used a specialized test fixture that forced bars of material into the splaying mode, which is not necessarily what occurs naturally in tubes made from chopped fiber material systems [3] [4]. The research also showed that the energy absorption results depended upon the boundary conditions set on the test fixture [5]. Turner et al. have completed the most comprehensive study of discontinuous fiber tubes found in literature to date [6]. However, their work focused on specific energy absorption and did not detail failure morphology. As such, there is not currently an associated failure morphology with the crush response of prepreg platelet molding compound tubes. This work will provide a failure morphology characterization in order to fill gaps in literature.

Load-Displacement Curve

The physical quantities measured during crush experiments are the load required to continue the crushing process and the displacement of the platens on the test fixture. From these quantities the load-displacement curve can be created and provide a significant amount of information regarding the crush response of the component.

A typical load-displacement curve can be seen in Figure 2. The figure is divided into five stages corresponding to typical phases of loading during crushing of composite tubes [7]. At the start of the test, the tube will begin to take load, which is evident by a linear slope. During this time, the trigger installed on the tube via bevel, notch, or ply drop off may be crushing. This initiates a progressive failure where the tube crushes steadily from the top down, instead of a catastrophic failure where the tube breaks somewhere in the middle and no longer takes load. The peak load, designated by a *1* on Figure 2, is attained when local fracture occurs on the tube at full thickness. A drop in load is observed afterwards, at point *2*, when the crash front is forming. Depending on the failure morphology, this drop in load is not always present. The size of the load drop is also dependent upon the type and angle of the trigger on the tube. The load gradually saturates again, point *3*, and eventually reaches the stable crushing load at point *4*. Stable crushing can have a cyclic response due to fiber bundles forming and breaking off or localized buckles forming. The splaying mode will provide a load-displacement curve that does not oscillate because failure propagation is dependent upon a constant load to cause further delamination. The stable crush zone, point *5*, is defined as the distance on the curve that maintains the stable crush load. Eventually the stable crush zone ends due to the tube being completely crushed or the crush event ending.

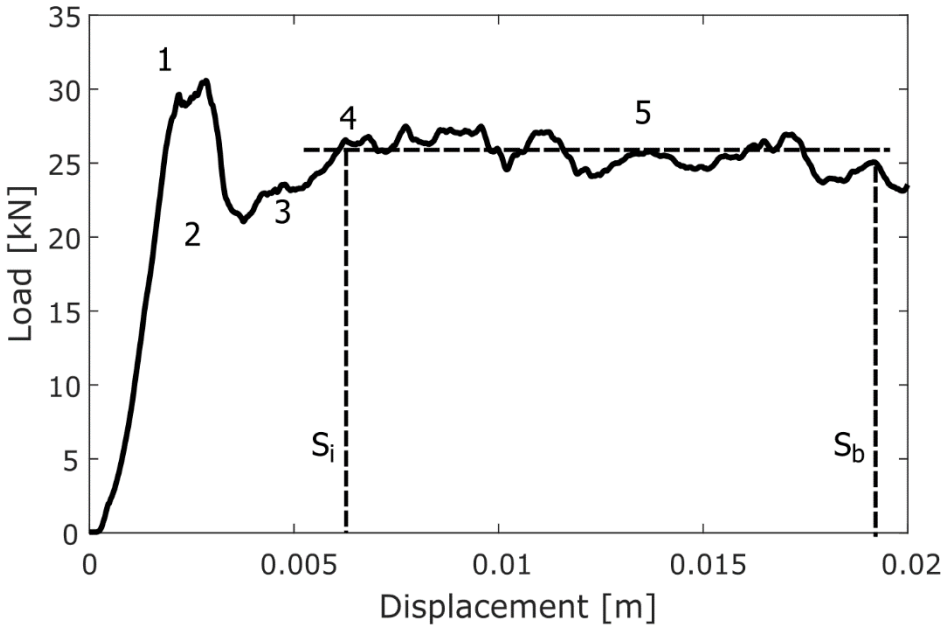

Figure 2: Characteristic load-displacement curve of a tube in crush recreated from Ramakrishna [6]

Changes to the layup will always change the load-displacement curve, even if the failure morphology stays the same. However, changes in failure morphology dramatically change the shape of the load-displacement curve. A high ratio of axial fibers, that produces the splaying failure mode, will produce a large initial peak and lower stable crushing load. A tube with a high ratio of hoop fibers, that produces the fragmentation failure mode, will have a lower initial peak and oscillating jagged peaks from fiber bundles forming and breaking off the tube[1].

Specific Energy Absorption

The specific energy absorption (SEA) is the amount of kinetic energy absorbed per unit material during the test. The SEA is calculated with data from the stable crush zone portion of the test.

Starting with the total work done on the system

$$U = \int_{S_i}^{Sb} P dS \tag{1}$$

Where U is the energy absorbed, S_i and S_b are crush distances corresponding to the beginning and end of the stable crush zone, and P is the load measured during the crushing process. From there, the specific energy absorption can be defined as the energy absorbed per unit material. Using the average stable crush load, $\bar{P}$, allows for the removal of the integral and produces the following

$$SEA = \frac{U}{m} = \frac{\bar{P}(S_b - S_i)}{V\rho} = \frac{\bar{P}(S_b - S_i)}{AL\rho} \tag{2}$$

Where V is the volume that breaks down to area, A, multiplied by length, L, of the cross section, and ρ is the density of the material.

Assuming the specific energy absorption is not dependent upon the current location in the stable crush zone, the SEA can be further reduced to a final form of

$$SEA = \frac{\bar{P}}{A\rho} \tag{3}$$

The SEA gives a comparative value for the overall crush performance of a material system. A high specific energy absorption is desirable for a material system because it becomes a viable option for use in the automotive industry for crash applications.

Manufacturing Methods

This prepreg platelet molding compound is created by slitting and chopping continuous fiber prepreg and letting the newly formed platelets drop onto nonstick film on a moving line. The system is then compressed and heated slightly to ensure the platelets stick together and can be handled without falling apart. The thermoset material system is delivered to Purdue in rectangular sheets of PPMC. An example of this can be seen in Figure 3.

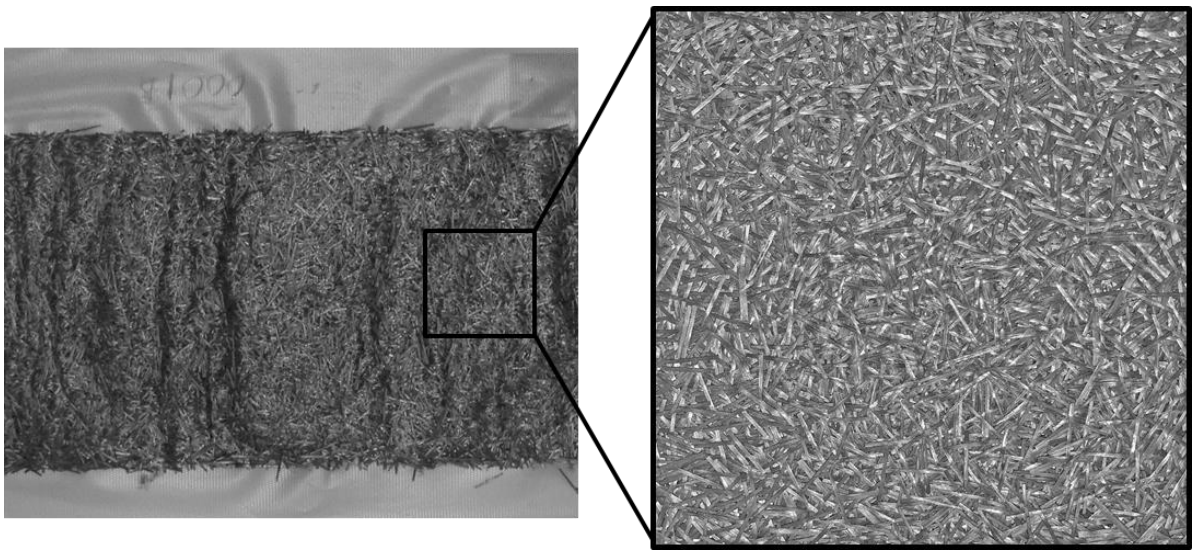

Figure 3: Prepreg platelet molding compound

Heat Shrink Manufacturing Method

Two manufacturing methods were created to fabricate carbon fiber tubes with the VORAFUSE M6400™ material system. The first method implemented used a hollow aluminum mandrel that was 50.8 mm in outer diameter. A 254 mm x 254 mm sheet of composite material was wrapped around the mandrel, after mold release had been applied. The material is not tacky at room temperature, so a heat gun was used to make the easier for rolling. Continuous fiber unidirectional layups were created with this manufacturing method because it prevented pinching and wrinkling of the prepreg. However, a few samples of the PPMC tubes were also created with this method. A sheet of silicone rubber was then wrapped around the composite material for one revolution.

Heat shrink tape was applied in overlapping layers along the length of the tube twice. A wrapping force of about 30N was the goal when rolling the heat shrink tape on to the mandrel. The entire setup was placed in an oven at 180°C for 30 minutes. A schematic of the heat shrink manufacturing method can be seen in Figure 4.

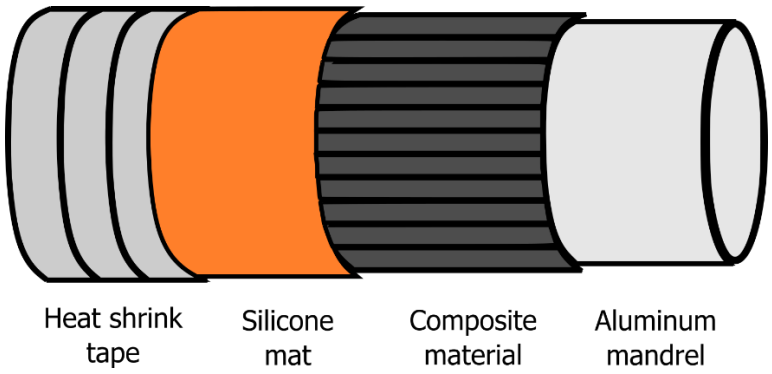

Figure 4: Schematic of heat shrink manufacturing method

Tubes produced with the heat shrink method had smooth inner surfaces, but significant texture on the exterior surfaces. This is in part because the material was pressurized from the outside in, and the heat shrink tape did not provide a smooth surface for the tube to form to. Figure 5 shows a manufactured unidirectional tube on the left and a PPMC tube on the right. The unidirectional tube has resin rich ridges that were formed due to the overlaps of the heat shrink tape. The PPMC tube has a textured surface with ridges corresponding to individual platelet orientation.

Figure 5: Manufactured tubes from heat shrink method; unidirectional prepreg (left) PPMC (right)

Mold Manufacturing Method

Bladder molding was the second manufacturing process for the PPMC tubes. A two-part tube mold was 3D printed out of thermoplastic PPS at the Purdue Composites Manufacturing and Simulation Center. This mold contains a cavity for a 50.8 mm outer diameter cylinder that is 300 mm in length. A custom perforated, steel mandrel was manufactured with an outer diameter of 44.45 mm. The mandrel was closed on the ends with a compressed air line nozzle attached on one end. The mandrel has hundreds of 3.175 mm holes drilled into the cylindrical surface to allow air from the compressed airline to flow out of the mandrel. During manufacturing, a 48 mm outer diameter silicone tube provided by Torr Technologies was slid onto the mandrel, and 54 mm outer diameter square cross sectional O-rings were used to compress the silicone tube against the mandrel and prevent air from escaping. A sheet of the PPMC was wrapped on top of the silicone tube, and the entire mandrel setup was placed inside of the mold during manufacturing. A schematic of the setup can be seen in Figure 6.

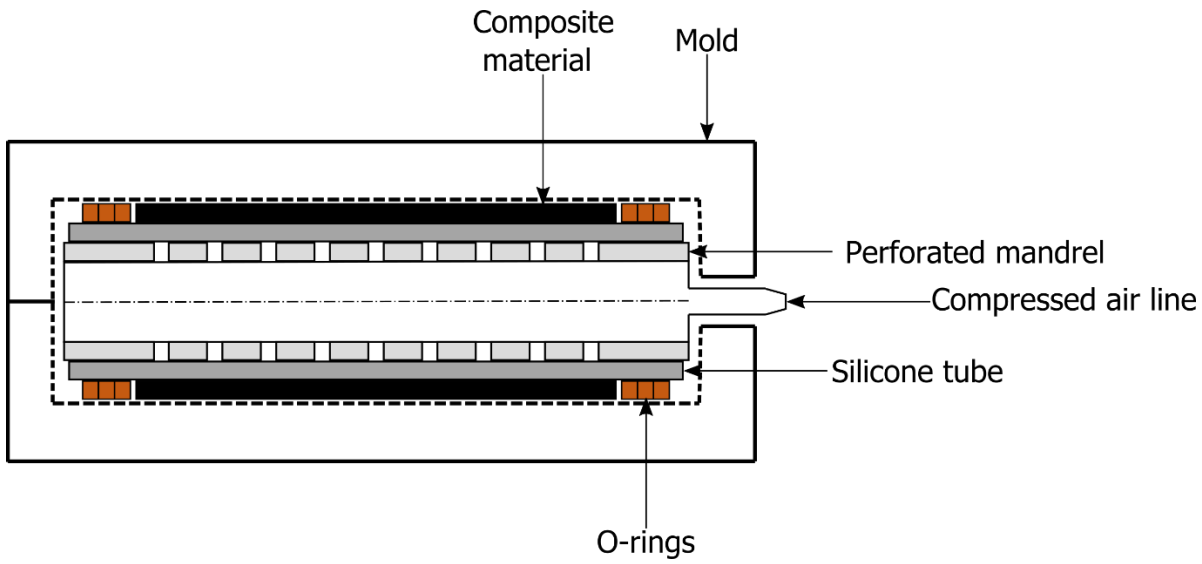

Figure 6: Schematic of manufacturing setup for PPMC tubes

The manufacturing process started by heating the two-part mold in an oven at 180°C for 30-40 minutes. At the same time, the platens on the press were pre-heated to a temperature of 180°C. The mandrel was prepared by cleaning the silicone tube and sliding the tube onto the mandrel. A 254 mm x 254 mm PPMC mat was thawed, and a heat gun was used to make the prepreg platelet mat more malleable and tacky in order to get the thick sheet rolled onto the mandrel. The PPMC sheets were not consistent in thickness, but averaged between 2-2.5 mm. Once the PPMC was rolled, a series of O-rings were slid over the silicone tube and mandrel without touching the composite material. The mold was removed from the oven, the mandrel assembly was placed in the mold, and the mold was closed. The completed mold was then placed inside the 30-ton press, and was compressed with 19 kN of force. An air line was connected to the compressed air nozzle sticking out of the mold, and the bladder was pressurized to 100 psi or 0.7 mPa. The mold remained in this configuration for 30 minutes, and then the bladder was deflated, and the mold was removed from the press.

A demolded tube has flash and some pinched material present along the seams of the mold,

an example of this be seen in Figure 7. The pinched PPMC material does not result in wrinkling of the tube like it would for continuous fiber layups. In this case the tube was pressurized from the inside pushing out resulting in a smooth outer surface that was forced against the mold walls. However, the interior of the tube now has a surface texture similar to the exterior of the heat shrink tubes that depend on platelet overlapping and orientations. The manufactured tubes are cut with a tile saw to produce two 100 mm long test samples. The flash and pinched material are sanded off to create a flush surface.

Figure 7: Demolded tube prior to finishing

TEST METHOD

Prior to testing, a bevel was machined into one end of each test sample at roughly a 45° angle. The bevel acts as a crush initiator to ensure the tube will fail at the beveled end first and will trigger a progressive crush response. The tubes were spray painted white and were given a black speckle pattern for capturing digital image correlation data (DIC) on the tubes during testing.

Testing was completed on a 100 kN MTS machine that had flat platens on the crossheads. The crush rate was set to a quasi-static speed of 4 mm/s, and the tubes were crushed a distance of 40 mm. The load and displacement signals were recorded at a sample rate of 200 Hz. A two-camera DIC setup was used to capture video of the failure at 20 frames per second.

MICROSCOPY

Seventeen total samples were produced from 8 manufactured tubes, and sections from each tube were reserved for microscopy. These included 2 samples of an axial $[0_{14}]$ continuous fiber layup, 3 samples of a hoop $[0_2/90_{14}]$ continuous fiber layup, and 3 samples of PPMC tubes all made with the heat shrink method. In this case, a $0°$ ply aligns the fibers along the longitudinal axis of the tube. After that, 9 samples of PPMC tubes were made with the molding manufacturing method.

The $[0_{14}]$ samples produced from the heat shrink method averaged 3.78 mm in thickness while the $[0_2/90_{14}]$ averaged 2.97 mm, and the PPMC tubes averaged 2.24 mm. The test specimens from the mold method averaged 2.04 mm in thickness with a 0.15 mm standard deviation. There was significant variation in thickness along the hoop direction of all the tubes. Therefore, six thickness measurements were made along the top and bottom of each test sample. The largest standard deviation for thickness measurements made on a single tube was 0.5 mm, which is about 25% of the tube thickness. These thickness variations are not insignificant and are considered going forward.

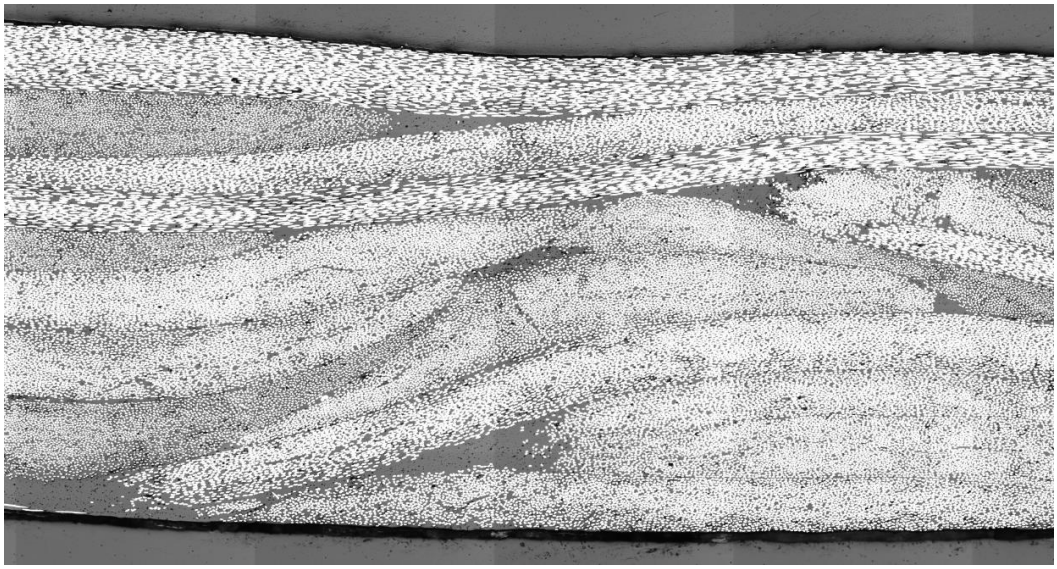

Figure 8: Cross section looking down longitudinal axis of PPMC molded tube

Under a microscope, distinct platelets can be seen, and this is evident in Figure 8. This micrograph shows the cross section of a molded PPMC tube looking down the longitudinal axis. Resin rich areas appear at the ends of the platelets as well as at the border of the tube itself. Waves formed by the platelets are present through the thickness of the tube and also seen on the inside edge of the tube where the bladder applies pressure. This waviness explains the variations in thickness around the circumference of the part and the rough texture on the inside of the tube.

FAILURE OF PREPREG PLATELET TUBES

Failure Morphology

In general, the progressive failure of the PPMC tubes showed characteristics of both the splaying and fragmentation continuous fiber failure modes. An example of the failure morphology

can be seen in Figure 9, and a stitched micrograph of a representative failure site is shown in Figure 10. Delamination occurred between platelets, and large sections of debris curled off from the tube in a splaying fashion. A wedge of debris helped the delamination process extend further down the tube. During the tests, small platelet bundles also broke off the tubes and fell away. The bundles from the PPMC tubes are likely discrete platelets breaking off. Figure 10 specifically shows delamination between platelets as well as the debris and fragments that have broken off of the tube.

Figure 9: Example failure morphology of crushed PPMC tube

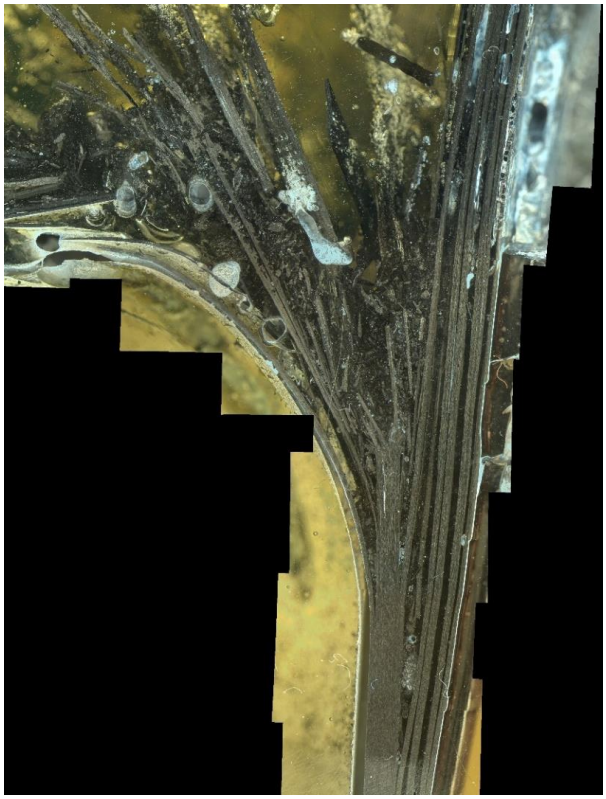

Figure 10: Stitched micrograph of PPMC tube crush failure

Load-Displacement Curve

Figure 11shows a load-displacement curve for a single PPMC tube. There is not a significant initial peak that would be seen with a continuous fiber splaying mode. Instead, there is a small initial peak followed by a drop in load and then oscillatory behavior around a stable crushing load. The oscillatory behavior with random jagged peaks is consistent with a continuous fiber fragmentation failure mode.

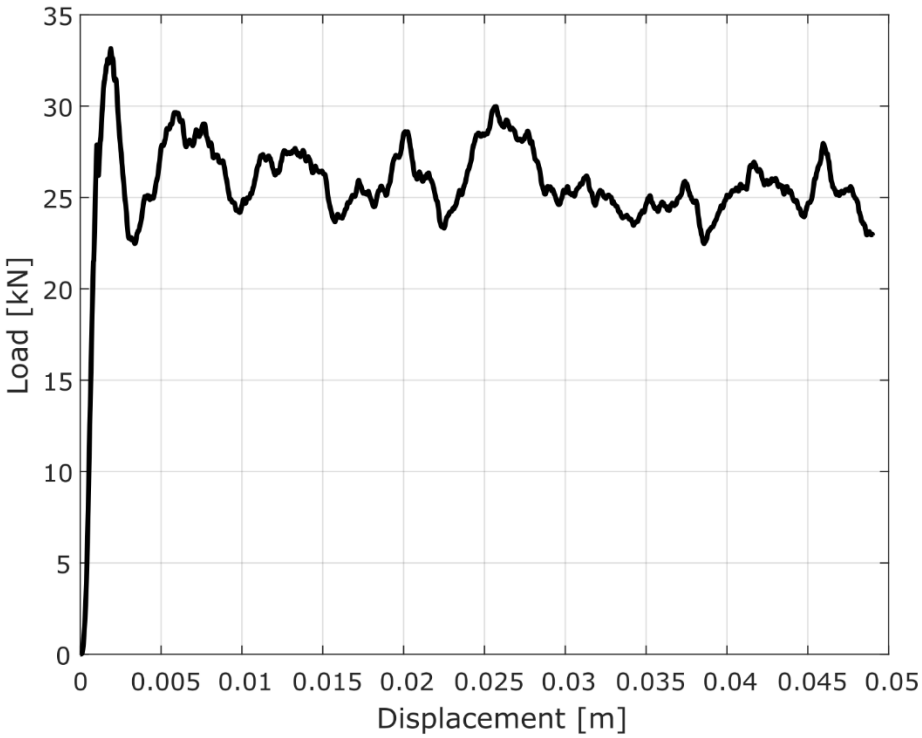

Figure 11: Single load-displacement curve

The load-displacement curves were averaged across the 9 samples made from the molding method, and this averaged response can be seen in Figure 12. The gray area is associated with the first standard deviation of the averaged response. Comparing the averaged response to the representative response in Figure 11 shows the consistency of the shape of the load-displacement curve for the PPMC tubes. While there was spread in stable crushing load and peak load, these can be attributed to manufacturing parameters, bevel specifications, and orientation variability throughout the prepreg platelet molding compound. Samples produced from the same tube had consistently similar results. This could indicate manufacturing variabilities play more of a role in performance than the platelet orientation variability.

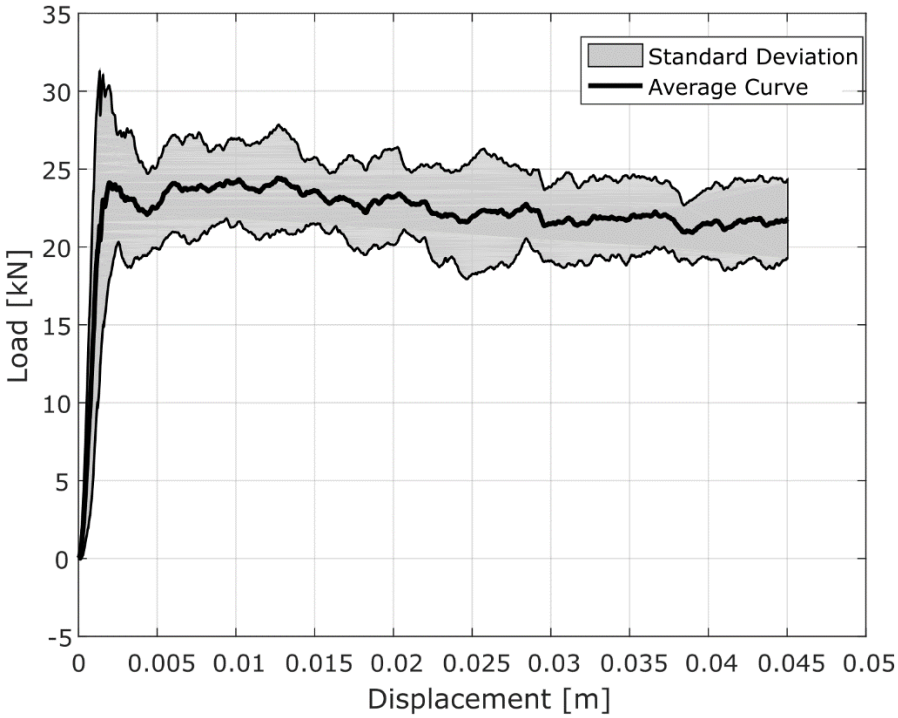

Figure 12: Average load-displacement curve for PPMC tubes from molding method

Specific Energy Absorption

The specific energy absorption calculated for the molding method samples averaged to 42.3 kJ/kg with a standard deviation of 4.7 kJ/kg. The maximum difference of SEA between all of these tubes was around 13 kJ/kg, however, the largest spread among two samples from the same manufactured tube was only 2.07 kJ/kg. This again emphasizes the consistency of performance for samples from the same tube and that manufacturing parameters may have the largest effect on performance.

Comparison of Prepreg Platelet Tubes to Continuous Fiber Tubes

Failure Morphology

Figure 13 provides a table comparing the expected failure morphology from literature and the failure morphology obtained in lab from the manufactured crush tubes. The drawings of the splay and fragmentation failure modes are recreated from work by Hull [1]. However, there is not a failure representation of PPMC tubes available in literature, therefore the drawing of the PPMC failure is original. It is clear that the continuous fiber tube failures matched expectations from literature.

As previously stated, the PPMC failure resembles a splaying mode. However, the PPMC morphology differs from continuous fiber splaying mode because the splay sections are larger and produce fewer splayed fiber bundles. The radius of curvature associated with these splayed sections is also smaller. This is likely due to the decreased bending stiffness of the PPMC compared to an axial fiber dominated layup seen with the splaying mode in the continuous fiber

tubes. The bundles breaking off of the PPMC tubes are similar to the fragmentation mode seen with continuous fibers. However in the continuous fiber case, the fiber bundles span the entire circumference of the tube, forming rings. The PPMC platelets that break off are smaller and more representative of debris flakes than rings.

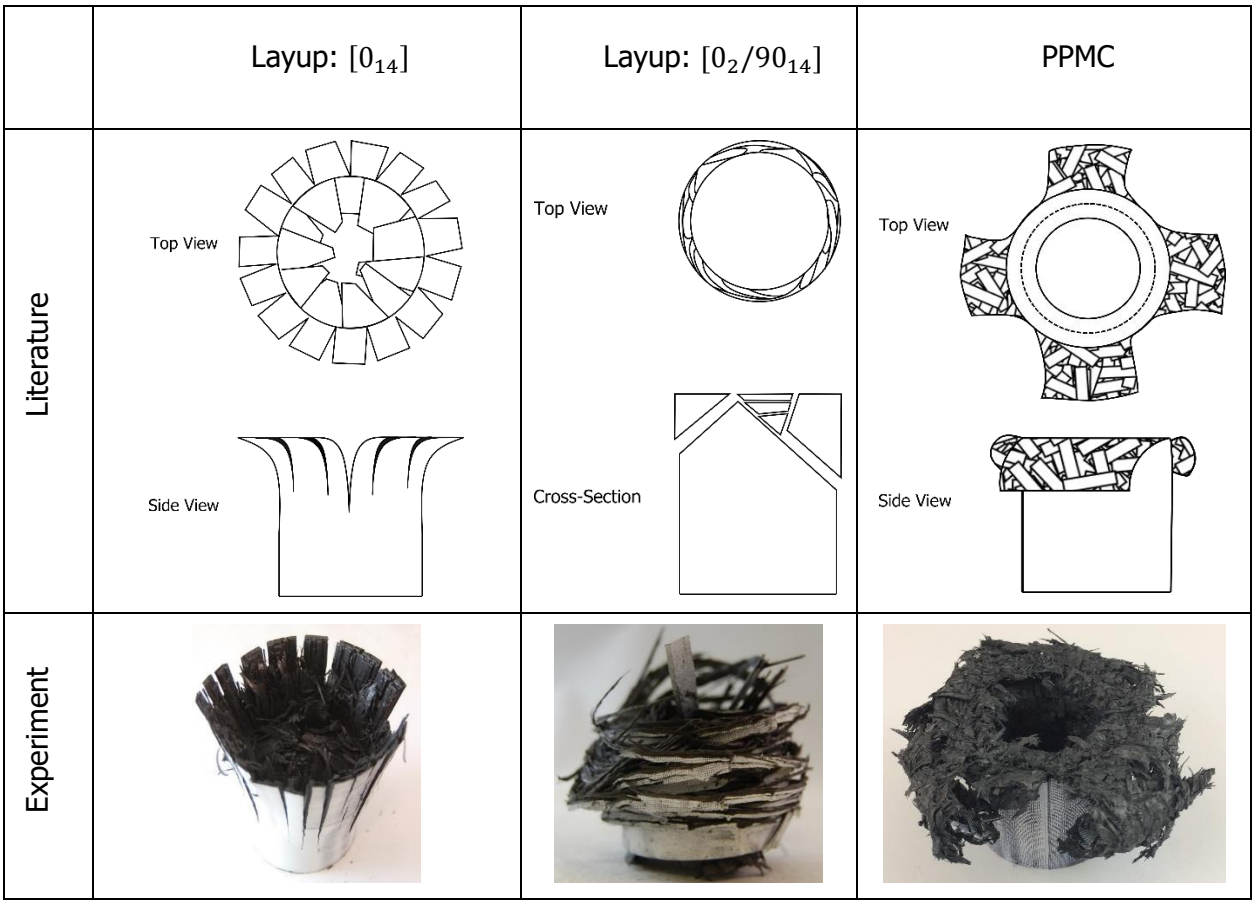

Figure 13: Failure morphology comparison of continuous fiber and PPMC tubes

Load-Displacement Curve

Load-displacement curves produced by the 3 different tube types can be seen in Figure 14. The $[0_{14}]$ tube had a large initial peak followed by a significant drop in load. The stable crushing load then continued on at a significantly lower value. The $[0_2/90_{14}]$ tube produced a lower initial peak than the axial tube. However the stable crushing load was consistent with the initial peak and there was no significant drop in load. Instead, oscillations with jagged features characterized the failure as individual fiber bundles took load and then broke off. The PPMC tubes resembled a shape more likely to be seen with the fragmentation failure mode than the splay failure mode for continuous fibers.The initial peak was on par with the stable crushing load, however there was a slight drop in load after the first peak before the load saturated again. There were oscillations in the stable crush zone, but they were not as severe compared to the $[0_2/90_{14}]$ case. The initial slopes of the $[0_{14}]$ tube and the PPMC tubes were almost identical while the $[0_2/90_{14}]$ tube had a lower slope. The initial slope is dominated by effects of the trigger, so it is likely the bevel was not consistent between all of the tubes causing slight differences. There was not a significant

difference seen in load-displacement curves for PPMC tubes created from either manufacturing method. From this plot alone, a case could be made that the PPMC tubes perform as well as some unidirectional layups in crush.

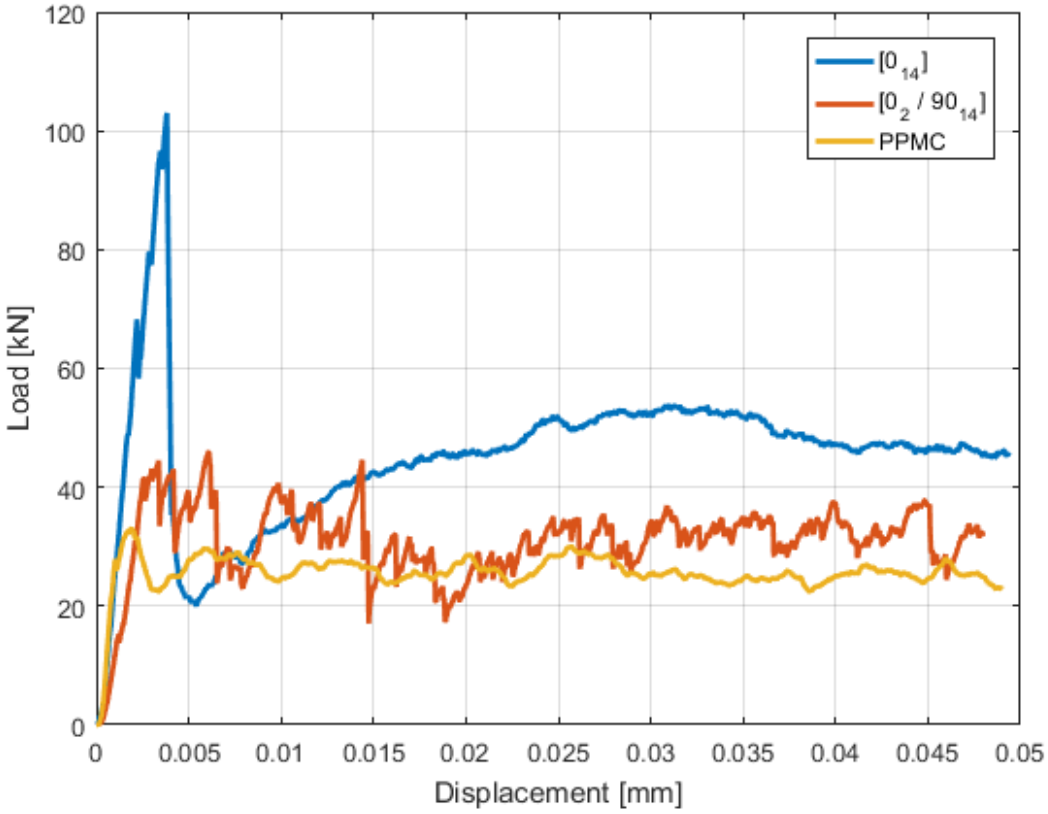

Figure 14: Load-displacement curve comparison between tube types

Specific Energy Absorption

The specific energy absorption for each of the manufactured tube types was calculated using Eq. 3 and the spread of these values can be seen in Figure 15. As is evident from the red lines in the figure, the average SEA for the different tube types are all within 3 kJ/kg of each other. The heat shrink PPMC tubes had the highest average SEA at 44.08 kJ/kg, followed by the 43.08 kJ/kg for the $[0_2/90_{14}]$ tubes. The molded PPMC tubes had an average SEA of 42.3 kJ/kg, and the $[0_{14}]$ tubes had the lowest average at 41.72 kJ/kg. However, in order to get a better comparison, more samples need to be tested, especially of the continuous fiber layups. Even with the smaller sample size, these results do tell us that the PPMC tubes perform as well as some unidirectional layups of the same material in crush. This implies that PPMC could be a viable alternative to traditional composite materials for performance in crash.

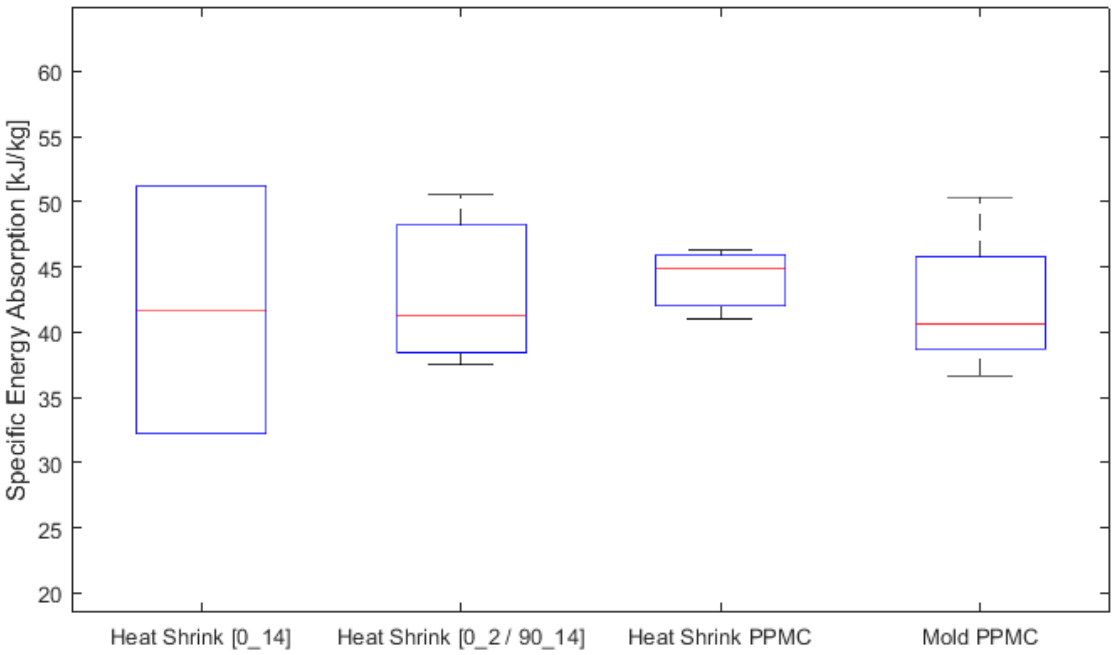

Figure 15: Specific energy absorption comparison between layup and manufacturing method

Summary and Next Steps

Seventeen crush tubes made of VORAFUSE M6400™ were manufactured with a heat shrink process or a bladder molding procedure. Each of the samples was tested in crush to investigate progressive failure of the PPMC material system and compare it to traditional unidirectional layups. The failure morphology of the PPMC tubes showed characteristics of a splaying failure mode mixed with platelet bundles breaking off as is common in fragmentation failure modes. The load-displacement curves produced by these samples mimicked a response often seen in the fragmentation failure mode in continuous fiber crushing. The specific energy absorption average was 42 kJ/kg for molded PPMC tubes, and that was within 3 kJ/kg of the unidirectional layups also tested. These results indicate that the PPMC performs as well as some unidirectional layups.

Future plans include manufacturing more PPMC tubes at a variety of processing conditions to identify manufacturing parameters that affect the crush performance. Additional continuous fiber tubes with different layups will be manufactured to better determine how well the PPMC performs compared to continuous fiber. A study into the effect of platelet orientation on specific energy absorption will be performed as well to understand variability in the failure response.

Acknowledgements

This work was sponsored by the Institute for Advanced Composites Manufacturing Innovation under Project 3.2. In addition, thanks to Torr Technologies for providing the silicone tubes used for bladder molding.

Bibliography

1. D. Hull, "A Unified Approach to Progressive Crushing of Fibre-Reinforced Composite Tubes," *Composites Science and Technology,* vol. 40, pp. 377-421, 1991.

2. G. L. Farley and R. M. Jones, "Crushing Characteristics of Continuous Fiber-Reinforced

Composite Tubes," *Journal of Composite Materials,* vol. 26, no. 1, pp. 37-50, 1992.

3. G. C. Jacob, J. M. Starbuck, J. F. Fellers and S. Simunovic, "Crashworthiness of Various Random Chopped Carbon Fiber Reinforced Epoxy Composite Materials and Their Strain Rate Dependence," *Journal of Applied Polymer Science,* vol. 101, pp. 1477-1486, 2006.

4. G. C. Jacob, J. M. Starbuck, J. F. Fellers and S. Simunovic, "Effect of Fiber Volume Fraction, Fiber Length and Fiber Tow Size on the Energy Absorption of Chopped Carbon Fiber Polymer Composites," *Journal of Polymer Composites,* vol. 26, pp. 293-305, 2005.

5. G. C. Jacob, J. M. Starbuck, S. Simunovic and J. F. Fellers, "New Test Method for Determining Energy Absorption Mechanisms in Polymer Composite Plates," *Polymer Composites,* vol. 24, no. 6, pp. 706-715, 2003.

6. T. Turner, L. Harper, N. Warrior and A. Caliskan, "Energy Absorption Performance of Meso-Scale Discontinuous Carbon Fibre Composites," *International Journal of Vehicle Structures and Systems,* vol. 3, no. 2, pp. 80-86, 2011.

7. S. Ramakrishna and H. Hamada, "Energy Absorption Characteristics of Crash Worthy Structural Composite Materials," *Key Engineering Materials,* Vols. 141-143, pp. 585-622, 1998.